Available at www.sciencedirect.com

ScienceDirect

journal homepage: www.elsevier.com/locate/he

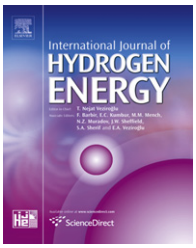

Synthesis and characterization of high-density non-spherical $Ni(OH)_2$ cathode material for Ni–MH batteries

Enbo Shangguan [a], *Zhaorong Chang* [a,*], *Hongwei Tang* [a], *Xiao-Zi Yuan* [b], *Haijiang Wang* [b]

[a] *College of Chemistry and Environmental Science, Henan Normal University, Xinxiang 453007, PR China*
[b] *Institute for Fuel Cell Innovation, National Research Council of Canada, Vancouver, BC V6T 1W5, Canada*

ARTICLE INFO

Article history:
Received 19 April 2010
Received in revised form
22 June 2010
Accepted 28 June 2010
Available online 3 August 2010

Keywords:
Nickel hydroxide
High tap-density
Drying method
Ni–MH batteries
Cathode materials

ABSTRACT

Positive electrode active materials of non-spherical nickel hydroxide powders with a high tap-density for alkaline Ni–MH batteries have been successfully synthesized using a polyacrylamide (PAM) assisted two-step drying method. The tap-density of the powders reaches 2.32 g cm^{-3}, which is significantly higher than that of nickel hydroxide powders obtained by the conventional co-precipitation method. X-ray diffraction (XRD), infrared spectroscopy (IR), scanning electron microscopy (SEM), thermogravimetric/differential thermal analysis (TG-DTA), Brunauer–Emmett–Teller (BET) testing, laser particle size analysis, tap-density testing, cyclic voltammetry (CV), electrochemical impedance spectroscopy (EIS), and a charge–discharge test were used to characterize the physical and electrochemical properties of the synthesized material. The results show that the as-prepared nickel hydroxide materials have an irregular tabular shape, a high density of structural disorder, and a high specific surface area. The charge–discharge tests indicate that nickel hydroxide powders synthesized by the new method have better electrochemical performance than those obtained by the conventional co-precipitation method. This performance improvement could be attributable to a more compact electrode microstructure, a lower amount of intercalated anions, better reaction reversibility, a higher proton diffusion coefficient, and lower electrochemical impedance, as indicated by TG-DTA, CV, and EIS. The results clearly show that better electrochemical activity can be achieved using nickel hydroxide that has a higher tap-density. Moreover, the new synthesis process is simple, cost-effective, and facile for large-scale production.

1. Introduction

Nickel hydroxide ($Ni(OH)_2$) has drawn considerable interest among materials chemists and battery technologists for its functionality as a cathode material in all nickel-based alkaline secondary cells [1–3]. It has been established that the physical properties of nickel hydroxide, such as its morphology, particle size distribution, tap-density, and specific surface area, are very important for its practical application in nickel batteries [4,5]. Because of its high tap-density and excellent electrochemical performance, spherical nickel hydroxide has been widely used as a cathode material in Ni–MH rechargeable batteries [6–11].

Generally, spherical nickel hydroxide can be prepared by a "controlled crystallization" method using $NiSO_4$, NaOH, and $NH_3 \cdot H_2O$ [6,7]. However, the preparation procedures are complex, the precipitated nickel hydroxide is allowed to age for a long time, the product quality cannot be easily

* *Corresponding author*. Tel.: +86 373 3326335; fax: +86 373 3326336.
E-mail address: czr_56@163.com (Z. Chang).
0360-3199/$ – see front matter © 2010 Professor T. Nejat Veziroglu. Published by Elsevier Ltd. All rights reserved.
doi:10.1016/j.ijhydene.2010.06.096

guaranteed, and the production cost is high. Hence, a simpler and more economical method of synthesizing nickel hydroxide cathode material with high volumetric energy density is required.

The conventional co-precipitation procedures for non-spherical nickel hydroxide powders are much simpler than those for spherical powders [12], are more economical because there is no hydroxide-forming step, and are more environmentally friendly because no ammonium is involved. Furthermore, the non-spherical powders have a large specific surface area and high electrochemical activity. To modify the structure and electrochemical performance of spherical nickel hydroxide, a high-energy ball milling method (HEBM) has been applied [13–15]. Compared with nickel hydroxide before HEBM, ball-milled nickel hydroxide possesses an irregular tabular shape, a higher surface area, smaller particle and crystallite sizes, more structural disorder, and higher electrochemical activity.

However, non-spherical nickel hydroxide powders always show a lower tap-density (1.5–1.8 g cm^{-3}) because of their irregular particle morphology and broad particle size distribution [12]. The low tap-density of the nickel hydroxide cathode material will result in a low volumetric specific capacity, thus seriously limiting the cell's energy density. Moreover, samples obtained by the conventional co-precipitation method are difficult to filter because of the suspended nickel hydroxide colloid, so improving the non-spherical nickel hydroxide powders' pile-density, usually the tap-density, is a serious challenge. Hence, the goal of this work is to seek a simpler method to synthesize high-density non-spherical nickel hydroxide.

In this study, a new polyacrylamide (PAM) assisted two-step drying method was proposed to prepare high-density non-spherical nickel hydroxide cathode materials. The physical and electrochemical properties of the prepared nickel hydroxide were characterized by means of X-ray diffraction (XRD), infrared spectroscopy (IR), and scanning electron microscopy (SEM), thermogravimetric/differential thermal analysis (TG-DTA), Brunauer–Emmett–Teller (BET) testing, laser particle size analysis, tap-density testing, cyclic voltammetry (CV), electrochemical impedance spectroscopy (EIS), and a charge–discharge test. It has been discovered that the prepared nickel hydroxide powder has a good electrochemical performance and a tap-density as high as 2.32 g cm^{-3}, which is the highest value known to date. The effect of tap-density on the electrochemical performance of nickel hydroxide electrodes is also discussed.

2. Experimental method

2.1. *Preparation of non-spherical $Ni(OH)_2$*

Stoichiometric amounts of $NiSO_4 \cdot 6H_2O$, were dissolved in distilled water to create a concentration of 1.67 mol L^{-1}. The aqueous solution was precipitated by adding a NaOH solution of 4 mol L^{-1} with continuous stirring at 50 °C. The co-precipitation mixtures were stirred continuously after the reaction ceased, and then coagulated by adding PAM (10 ml PAM (0.6%) per 200 ml solution), filtrated (under a pressure of 20 MPa), dried (at 120 °C for 2 h), ground, washed, and dried (at 120 °C for 2 h) to obtain a green sample (A). As this process involves two drying steps, the method is called PAM assisted two-step drying; the steps are summarized in Fig. 1. Using the same method, a second green sample (B) was obtained by changing the amount of added PAM (5 ml PAM (0.6%) per 200 ml solution) and the filtration pressure (10 MPa).

Nickel hydroxide was also synthesized by the conventional co-precipitation method. The starting materials and proportions were the same as used in the PAM assisted two-step drying method. The aqueous solution was precipitated by adding a NaOH solution of 4 mol L^{-1} with continuous stirring at 50 °C. The co-precipitation mixtures were stirred continuously after the reaction ceased, then filtrated, washed, and dried at 120 °C for 2 h in a vacuum drying oven to obtain sample (C).

2.2. *Characterization of non-spherical $Ni(OH)_2$*

The obtained powders were analyzed by XRD using a D8 diffractometer (Bruker, Germany) employing Cu Kα radiation. The scan data were collected in the 2θ range of 15–70°. The step size was 0.026° with a counting time of 3 s. The prepared powders were also observed using an SEM (SEM-6701F, JEOL, Japan), and the powders' components were obtained using a Fourier infrared spectrometer (FIRS; Bio-Rad FTS-40, US). TG-DTA was carried out using a Shimadzu DT-40 thermal analyzer (Japan). Measurements were performed in airflow using α-Al_2O_3 as the reference material.

A JZ-1 tap-density tester (China) was used to determine the tap-density of the sample as follows: 1) weigh the dried sample; 2) pour the weighed sample into the calibrated measuring cylinder; 3) install the cylinder into the tester and operate it until the volume ceases to decrease; and 4) read the volume. The specific surface area was evaluated by the BET nitrogen adsorption method using a 3H-2000 surface area analyzer (China). The particle size distribution of the powders was obtained using an OMEC LS-POP(III) particle size analyzer (China).

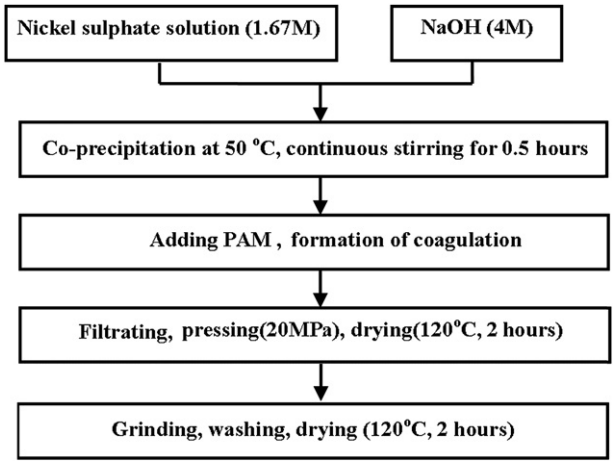

Fig. 1 – Synthetic route of the PAM assisted two-step drying method.

2.3. Nickel electrode preparation

Porous foamed nickel was cut into 2 cm × 2 cm squares to use as substrate material. The pasted nickel electrodes were prepared as follows: 80 wt.% nickel hydroxide, 10 wt.% nickel powder, and 5 wt.% carbon black were mixed thoroughly with a certain amount of 5 wt.% PTFE solution to obtain a homogeneous slurry possessing adequate rheological properties. The slurry was poured into a foam nickel sheet and dried at 80 °C for 5 h. Subsequently, the pasted electrodes were pressed at 20 MPa for 3 min to assure good electrical contact between the foam nickel and the active material.

2.4. Electrochemical measurement

Electrochemical tests were performed in a three-compartment electrolysis cell at ambient temperature. Two nickel ribbon counter electrodes were placed in the side chambers and the working electrode was positioned in the center. The electrolyte was a solution of 6 MKOH + 15 g L^{-1} LiOH. A Hg/HgO reference electrode was used via a luggin capillary, which was made in the same alkaline solution used in the working cell. CV and EIS were conducted on a Solartron SI 1260 impedance analyzer with a 1287 potentiostat interface. The CV test scan rate was between 1 mV s^{-1} and 8 mV s^{-1} and the cell potential ranged from 0.0 V to 0.8 V. For EIS, the impedance spectra were recorded at a 5 mV perturbation amplitude with a sweep frequency range of 10 kHz–1 mHz.

Test cells were assembled using the prepared nickel hydroxide electrode as the cathode, a hydrogen storage alloy electrode as the anode, and polypropylene to separate the cathode and anode. The electrolyte was a solution of 6 M KOH + 15 g L^{-1} LiOH. Charge/discharge measurements were conducted using a Land CT2001A battery performance testing instrument (China). For activation, three charge–discharge cycles at 0.1 C were performed, and the electrodes were discharged to 1.0 V. The discharge capacity of the nickel hydroxide in the positive electrode was based on the amount of active material ($Ni(OH)_2$) without taking into account the additives in the electrode.

3. Results and discussion

3.1. Physical characterization of $Ni(OH)_2$

The physical properties of nickel hydroxide samples A, B and C are listed in Table 1. The tap-densities of samples A and B, prepared by the PAM assisted two-step drying method, are 2.32 and 1.98 g cm^{-3}, respectively, remarkably higher than that of sample C obtained by the conventional co-precipitation method (1.62 g cm^{-3}). The mean diameters of samples A, B, and C are 28.20, 27.53, and 21.24 μm, and BET surface areas are 76.89, 83.26, and 105.15 m^2 g^{-1}, respectively.

These results show that the effect of the coagulating agent (PAM) on tap-density is significant. PAM is often used in water treatment, as it can be removed in the subsequent washing and drying process and does not affect the products. Adding an appropriate amount of PAM into the nickel hydroxide suspension greatly enhances the tap-density of nickel hydroxide powders by accelerating filtration rate and reducing the moisture content in the press cake. The effect may be attributable to the net structure formed when PAM is added, which results in agglomerations of colloid particles. Coagulation further increases the structure's density, as the agglomerations squeeze out water. Because of this dense structure, the nickel hydroxide particles are prone to grow and crystallize in the subsequent drying process, and the tap-density of the nickel hydroxide thereby significantly increases. Moreover, the products obtained using this new method are easy to filtrate because of the colloid particle agglomerations.

The XRD patterns of nickel hydroxide samples A–C are presented in Fig. 2. The characteristic diffraction peaks at (0 0 1)(d4.60), (1 0 0)(d2.70), (1 0 1)(d2.34), (1 0 2)(d1.76), (1 1 0)(d1.56), and (1 1 1)(d1.48) show that all these samples exhibit XRD characteristics of the β-$Ni(OH)_2$ phase with a brucite-type structure and a hexagonal unit. Some disorders in the crystal lattice, characterized by the full width at half maximum intensity (FWHM) of the (0 0 1), (1 0 1), and (1 0 2) reflection lines, can also be observed [16]. The FWHMs and the d-values of the respective samples in the (0 0 1), (1 0 0), and (1 0 1) diffraction lines are listed in Table 1. The interlayer distance c of a brucite-type structure of nickel hydroxide is represented by the $d_{0\,0\,1}$ value. The $d_{1\,0\,0}$ value corresponds to the Ni–Ni distance a in the layers of $Ni(OH)_2$, where $a = (2/\sqrt{3})d_{1\,0\,0}$ [17].

The broadening of some of the diffraction peaks [e.g., (0 0 1) and (h k 0)] is directly related to the crystallite size, D [30]. The crystallite size perpendicular to various diffraction planes can be estimated from the XRD lines using the Scherrer formula $D = 0.9\lambda/B\cos(\theta)$ (where D is the crystallite size, λ represents the X-ray wave length, B is the FWHM, and θ is the Bragg angle). As presented in Table 1, the FWHMs of the (0 0 1) and (1 0 0) diffraction lines tend to increase in the sequence A, B, C, indicating that the crystallite size of the nickel hydroxide powder tends to decrease, which is in accordance with the particle size results.

It has been pointed out that abnormal broadening of the (1 0 l) reflection lines ($l \neq 0$) cannot be attributed to crystallite size alone. Structural defects such as stacking faults, growth

Table 1 – Physical properties, FWHM and d-values in (0 0 1), (1 0 0), (1 0 1) diffraction lines of nickel hydroxide samples.

Sample	Tap-density/ g cm^{-3}	BET surface area/m^2 g^{-1}	Mean diameter/μm	(0 0 1)		(1 0 0)		(1 0 1)	
				FWHM/deg	d/nm	FWHM/deg	d/nm	FWHM/deg	d/nm
A	2.32	76.89	28.20	0.996	0.46793	0.852	0.27002	1.049	0.23393
B	1.98	83.26	27.53	0.997	0.46867	0.839	0.27058	1.034	0.23411
C	1.62	105.15	21.24	1.551	0.48050	1.002	0.27201	1.594	0.23629

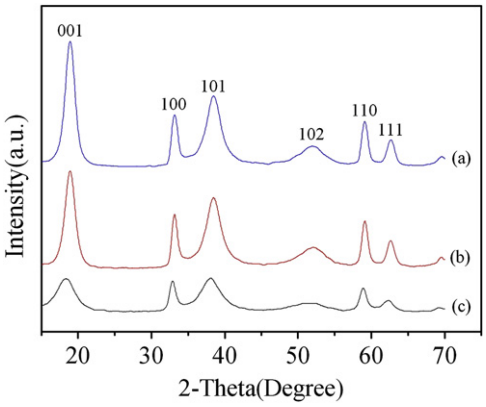

Fig. 2 – XRD patterns of samples A, B, and C.

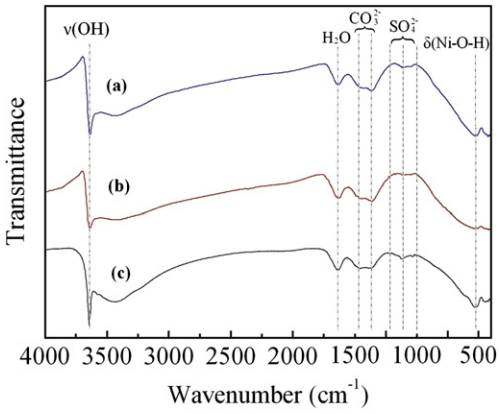

Fig. 3 – IR spectra of samples A, B, and C.

faults, and/or proton vacancies also play a very important role in explaining this broadening [18,19]. The (1 0 1) line shows a relationship with electrochemical activity, possibly due to the existence of stacking faults in the crystalline lattice of nickel hydroxide powders [20–23]. Structural disorder in nickel hydroxide can provide a better path for the diffusion of protons within the NiO layers and can help lower the free energy by increasing the entropy contribution, which can in turn increase the electrochemical reaction rate [11].

Köhler et al. [21] reported that less ordered nickel hydroxide materials characterized by an FWHM of the (1 0 1) line of 0.9 (2θ) or more exhibit a better specific capacity. The FWHMs of the (1 0 1) diffraction lines of samples A, B, and C are up to 1.049, 1.034, and 1.594, respectively, which indicates that all these samples possess a high density of structural disorder and better electrochemical activity. This result is attributed to the grinding, cutting, and deforming of large crystallites, which is similar to the high-energy ball milling method [13–15].

Fig. 3 presents the infrared spectra of the as-prepared samples A–C. Infrared spectra are useful for probing the short-range structure of nickel hydroxide, in contrast with the X-ray diffraction patterns that result from long-range phenomena. As is evident in Fig. 3, all three samples show similar characteristics. The strong, sharp band centered at 3640 cm^{-1} corresponds to the υO–H vibration, which is the typical IR spectra characteristic of β-$Ni(OH)_2$ [24]. The large bands around 3300 and 1650 cm^{-1}, due to the $\nu(H_2O)$ stretching vibration and the $\delta(H_2O)$ bending vibration of water molecules, indicate the presence of a certain amount of water molecules adsorbed on the nickel hydroxide [25]. These water molecules may play an important role in improving the rate-capacity performance of the nickel hydroxide electrodes by providing the passage for proton diffusion along the molecular chain between the layers [26]. The two low bands at about 1470 cm^{-1} and 1380 cm^{-1} in both IR spectra can be assigned to interference from the vibration of carbonate ions [27] due to the open system used for synthesis. The band at about 1125 cm^{-1} corresponds to the vibration of SO_4^{2-} [28]. The strong, narrow IR absorption band at 520 cm^{-1} can be ascribed to υNi–OH vibration, and the weak absorption band at 460 cm^{-1} is the υNi–O stretching vibration mode [29].

It was not possible to quantitatively determine from the XRD and IR studies the extent of hydration and the anions' intercalation in the various samples, so TG–DTA analyses were used to investigate the water content and dehydration reactions of the nickel hydroxide. The TG and DTA curves for nickel hydroxide samples A–C are shown in Fig. 4 and the experimental results are detailed in Table 2. All three samples

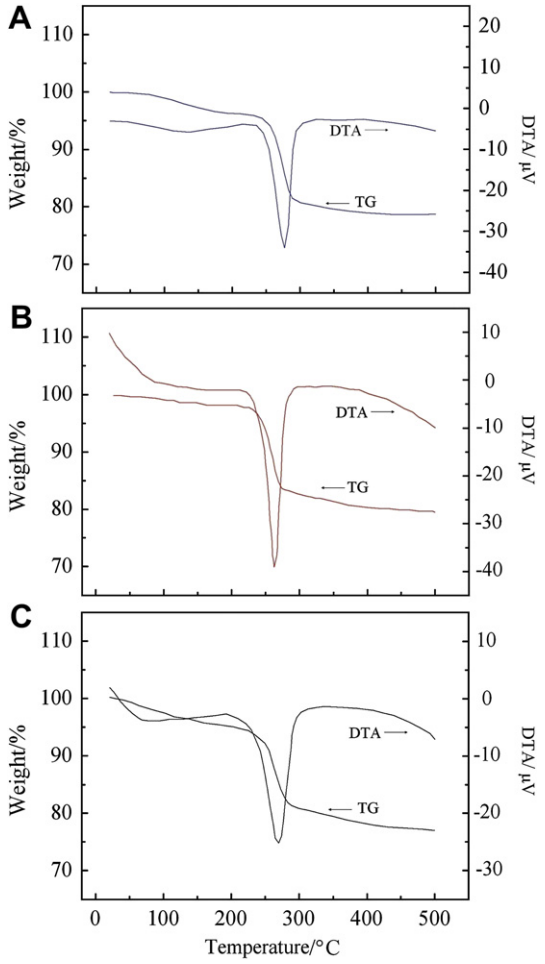

Fig. 4 – TG and DTA plots for $Ni(OH)_2$ samples A, B, and C.

Table 2 – Results of weight loss measurements for samples A, B, and C.

Weight loss region	Reason for loss	Sample		
		A	B	C
20–200	Dehydration (%)	3.42	2.85	5.42
200–350	Dehydroxylation (%)	17.0	15.98	13.87
350–500	Removal of intercalated anions (%)	0.83	2.21	3.82

show three weight loss regions. The first region is below 200 °C, where the adsorbed water is removed (Eq. (1)). The second is between 200 °C and 350 °C, where the samples decompose to NiO (Eq. (2)). The third is between 350 °C and 500 °C, where the intercalated anions are removed.Dehydration reaction:

$$Ni(OH)_2 \cdot X_{ads}H_2O \rightarrow Ni(OH)_2 + XH_2O \quad (1)$$

Decomposition reaction:

$$Ni(OH)_2 \rightarrow NiO + H_2O \quad (2)$$

In Eq. (1), the $H_2O/Ni(OH)_2$ molar ratio X_{ads} can be estimated from the weight loss corresponding to the dehydration reaction, and the nominal stoichiometric compositions of the nickel hydroxide samples are obtained. As presented in Table 2, the water content in samples A and B is relatively low compared to that in sample C. The X_{ads} values for the three samples were found to be 0.18, 0.15, and 0.30, respectively. Ramesh et al. [30] reported that the moisture content in nickel hydroxide is greatly dependent on the pH during precipitation. Thus, these results indicate that adding an appropriate amount of PAM under the same pH condition can greatly reduce the moisture content in the final product.

The theoretical weight loss corresponding to the decomposition reaction (Eq. (2)) is 19.43%, and the practical weight loss corresponding to this reaction, which can be estimated from the second weight loss steps of the TG curves, are 17.08%, 15.98% and 13.87% for samples A, B, and C, respectively. This indicates that the $Ni(OH)_2$ concentration (i.e., Ni composition) is higher in samples A and B than in sample C. The deviations between the practical and theoretical weight loss may be attributed to the SO_4^{2-} and CO_3^{2-} adsorbed in these materials, as revealed by IR analysis. The weight loss due to intercalation of anions was observed to be the highest for C (3.82%), whereas for A it was 0.83% and for B 2.21%. These results show that the nickel hydroxide powder obtained by the new method contains more Ni and fewer intercalated anions, which are likely boost its electrochemical activity.

In Fig. 4, it can be seen that the temperatures corresponding to the decomposition reaction peaks on the DTA curves gradually declines, with readings of 273.3, 265.2, and 261.8 °C for samples A, B, and C, respectively. This indicates that with decreasing tap-density, the synthesized nickel hydroxide materials become less thermally stable, as reflected in the higher decomposition reaction rate and lower decomposition temperature. That is, sample A with its higher tap-density has higher thermal stability than samples B and C.

Fig. 5 displays SEM photographs of samples A–C. All appear to be aggregates of irregular tabular shapes, similar to the ball-milled powders [13]. The irregular shapes may result from grinding, which leads to a higher specific surface area and more structural disorder, as shown in Table 1. In contrast to the typical spherical particles of β-$Ni(OH)_2$ [4,5], nickel hydroxide powders with irregular tabular shapes have a higher specific surface area that can provide a high density of active sites and thereby promote intimate interaction between the active material and the surrounding electrolyte [14,15].

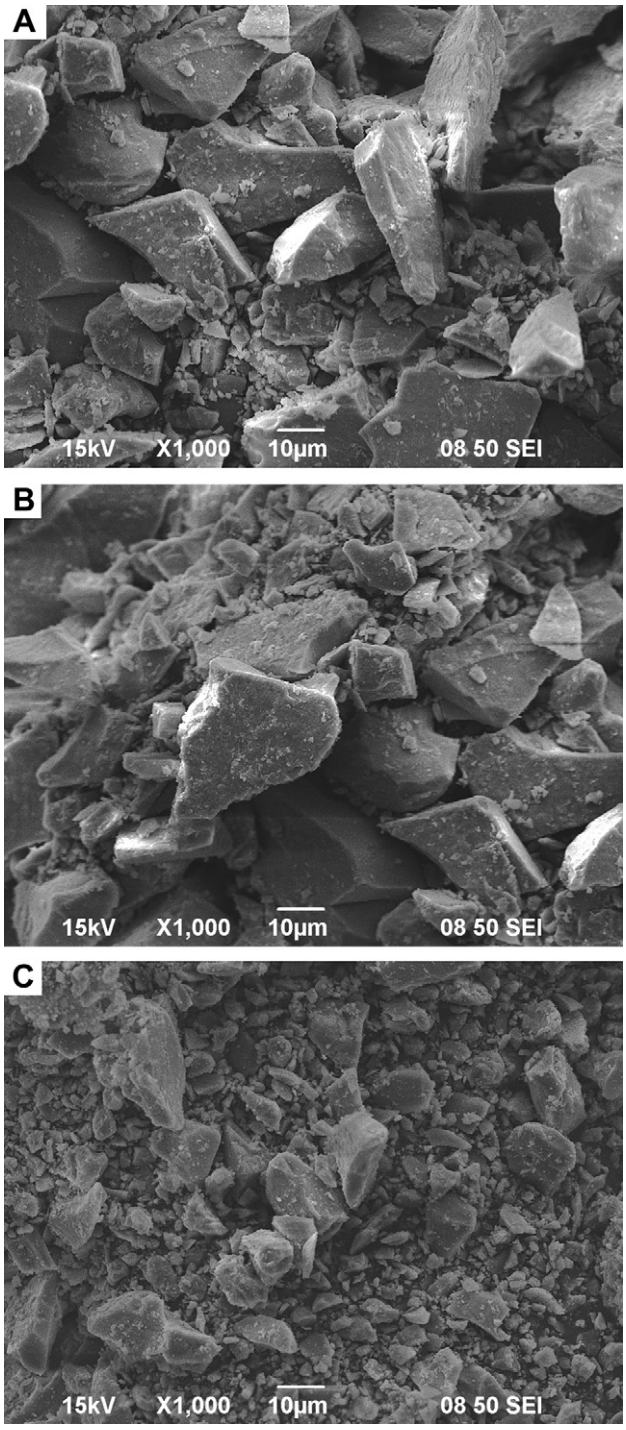

Fig. 5 – SEM images of $Ni(OH)_2$ samples A, B, and C.

3.2. CV and EIS measurements of nickel electrode

Fig. 6 illustrates the typical CV curves for samples A–C at various scan rates and 25 °C. For all the electrodes, at a scan rate of 1 mV s^{-1}, one anodic nickel hydroxide oxidation peak and one cathodic oxyhydroxide reduction peak are observable on the CV curves. As the scan rate increases from 1 to 8 mV s^{-1}, the oxidation and reduction peaks of samples A and B are clearly visible. However, for sample C, the oxidation peak disappears at scan rates above 6 mV s^{-1}, indicating an overlap between nickel hydroxide's oxidation peak and the oxygen evolution peak. Thus oxidation of nickel hydroxide to nickel oxyhydroxide will be accompanied by oxygen evolution, which in the early stage of charging will decrease charge efficiency and increase the pressure inside the battery.

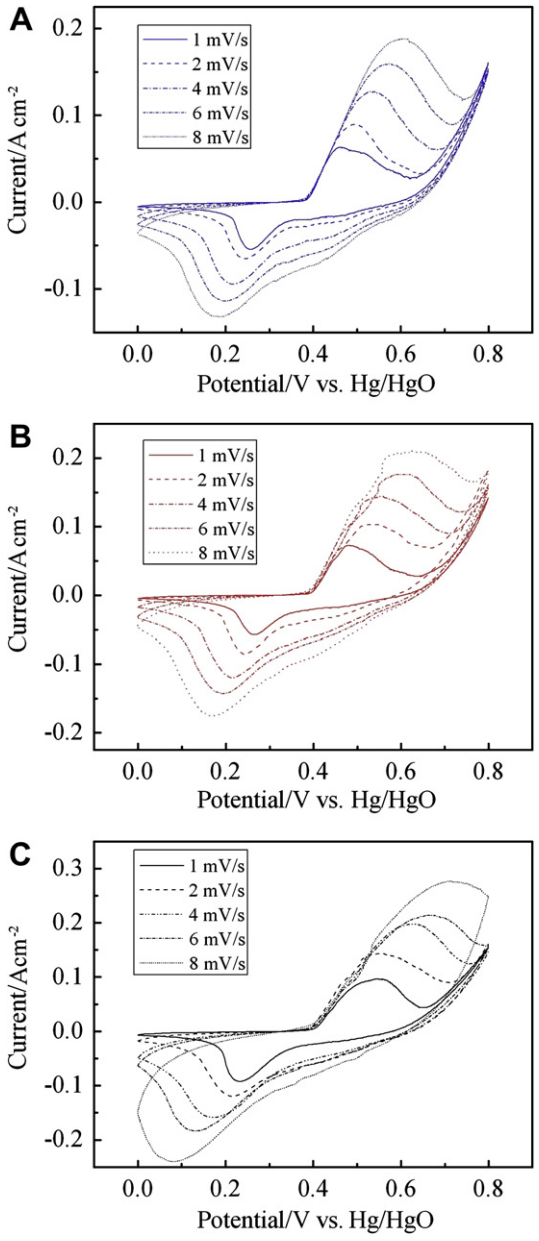

Fig. 6 – Cyclic voltammograms of samples A, B, and C at various scan rates.

Generally, the average of the cathodic and anodic peak potentials (E_{rev}) can be taken as an estimate of the reversible potential for nickel electrodes, and the potential difference ($\triangle E_{a,c}$) between the anodic (E_a) and cathodic (E_c) peak potentials is a measure of the reversibility of the redox reaction [11,31].

To compare the CV characteristics of electrodes A–C, the results of CV measurements at scan rate of 1 mV/s are tabulated in Table 3. The experimental data show that the redox reactions are somewhat quasi-reversible for all electrodes as indicated by the relatively large $\triangle E_{a,c}$. However, the $\triangle E_{a,c}$ of electrode A is only 202 mV, which is smaller than that of electrode B and C. This indicates that the charge and discharge process of the electrode A is better reversible, thus more active material can be utilized during charge and discharge, which is in accordance with the charge–discharge results as shown in Fig. 9.

It is well known that the electrochemical reaction process of a nickel hydroxide electrode is limited by proton diffusion through the lattice [32,33]. Therefore, it is of great importance to study the nickel electrode's proton diffusion coefficient. According to the Randles–Sevcik equation [32], at 25 °C the peak current, i_p, in the cyclic voltammogram can be expressed as

$$i_p = 2.69 \times 10^5 \times n^{3/2} \times A \times D^{1/2} \times C_0 \times \nu^{1/2} \quad (3)$$

where n is the electron number of the reaction (≈1 for β-Ni$(OH)_2$), A is the surface area of the electrode, D is the diffusion coefficient, υ is the scanning rate, and C_0 is the initial concentration of the reactant. For an $Ni(OH)_2$ electrode,

$$C_0 = \rho / M \quad (4)$$

where ρ and M are, respectively, the density and the molar mass (92.7 g/mol) of $Ni(OH)_2$.

Fig. 7 shows the relationship between the cathodic peak current (i_p) and the square root of the scan rate ($\nu^{1/2}$) for both nickel electrodes. The good linear relationship between i_p and $\nu^{1/2}$ confirms that the electrode reaction of $Ni(OH)_2$ is controlled by proton diffusion. Using the slope of the fitted line in Fig. 7 and Equation (3), the proton diffusion coefficient for sample A is calculated to be 6.81×10^{-10} cm^2 s^{-1}, which is comparatively larger than for samples B and C (5.92×10^{-10} cm^2 s^{-1} and 3.84×10^{-10} cm^2 s^{-1}).

Fig. 8 presents the electrochemical impedance spectra for electrodes A–C at steady state. The impedance spectra of all these electrodes display a depressed semicircle resulting from charge transfer resistance in the high-frequency region, and a slope related to Warburg impedance in the low-frequency region [34–36]. The impedance of electrode A is much smaller

Table 3 – Potential values of CV features for samples A, B, and C.

Sample	E_a/mV	E_c/mV	$\triangle E_{a,c}$/mV	E_{rev}/mV
A	259	461	202	360
B	255	476	221	366
C	233	542	309	388

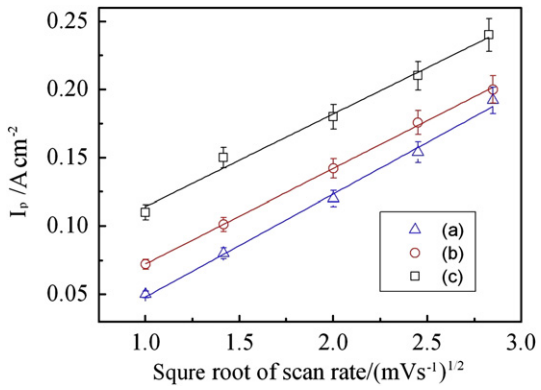

Fig. 7 – Relationship between the cathodic peak current (I_p) and the square root of the scan rate for samples A, B, and C.

than that of electrode B or C, which implies that the electrochemical reaction on electrode A proceeds more easily than on electrode B or C.

The higher proton diffusion coefficient and lower charge transfer resistance in high-density nickel hydroxide is attributable to fewer intercalated anions (e.g., SO_4^{2-}, CO_3^{2-}), more compact structure, high structural disorder density, and high specific surface area. The high density of structural disorder for nickel hydroxide powder is beneficial for the acceleration of solid-state proton diffusion in the $Ni(OH)_2$ lattice and will diminish the concentration polarization of protons during charge and discharge, leading to better charge–discharge cycling behaviour [14]. Moreover, non-spherical nickel hydroxide with a high surface area can provide a good interconnectivity network between the nickel hydroxide particles, and optimal degree of contact between the nickel electrode and the electrolyte, which can facilitate the rapid movement of electrons and ions in the electrode.

3.3. *Charge/discharge test of nickel electrode*

It is well known that adding cobalt compounds, such as metal cobalt, CoO, cobalt oxyhydroxide and cobalt hydroxide ($Co(OH)_2$), can significantly enhance nickel hydroxide utilization

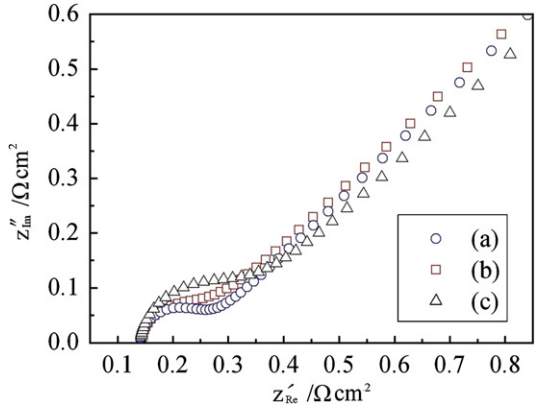

Fig. 8 – Electrochemical impedance spectra of samples A, B, and C.

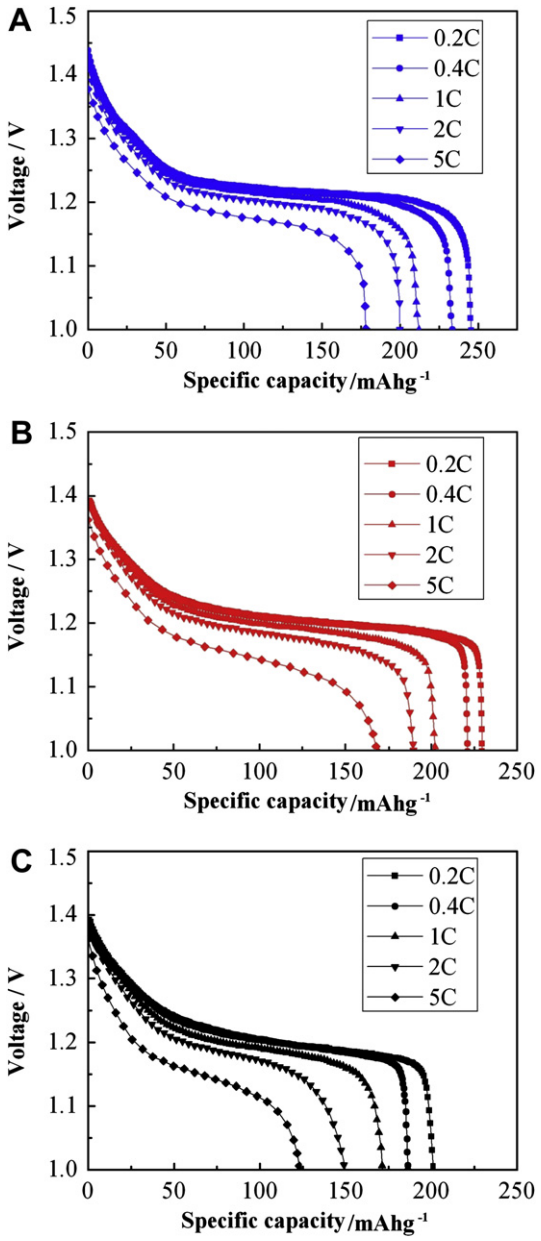

Fig. 9 – Discharge curves of the electrodes prepared with samples A, B, and C at different current rates.

[2, 37]. In order to study the effect of tap-density on the electrochemical performance of nickel hydroxide, nickel electrodes A–C were prepared without adding any cobalt compounds. Fig. 9 shows the discharge curves of nickel electrodes A–C at rates of 0.2, 0.4, 1, 2, and 5C, respectively. The experimental results are given in Table 4.

The specific discharge capacities of samples A and B, obtained by the new method, are both higher than that of sample C, prepared by the conventional co-precipitation method. At a rate of 0.2 C, sample A shows a volume capacity of 569.6 mAh cm^{-3}, which is 313.8 mAh cm^{-3} higher than that of sample C (255.8 mAh cm^{-3}). As the discharge rate increases from 0.2 to 5C, the discharge capacity of sample A decreases from 245.5 to 178.1 mAh g^{-1}, showing that at such a high

Table 4 – Results of charge/discharge test for different electrodes at different current rates.

Electrode	Specific capacity/mAh g^{-1}					Specific volume capacity/mAh cm^{-3}				
	0.2C	0.4C	1C	2C	5C	0.2C	0.4C	1C	2C	5C
A	245.5	233.6	212.1	199.9	178.1	569.6	542.0	492.1	463.8	413.2
B	229.7	221.1	201.3	189.7	168.2	454.8	437.8	398.6	375.6	333.0
C	201.1	186.4	171.6	150.5	123.7	325.8	302.0	278.0	243.8	200.4

discharge rate 72.5% capacity is retained. At the 5C rate, sample A shows a higher discharge capacity of 178.1 mAh g^{-1} and a volume capacity of 413.2 mAh cm^{-3}, whereas the values for sample C are 123.7 mAh g^{-1} and 200.4 mAh cm^{-3}, indicating that the high-rate performance of sample A is much better than that of sample C.

The cyclic performance of nickel electrodes A–C at the 1C rate is illustrated in Fig. 10.

The specific discharge capacity of electrode C decreased during the proceeding of the charge–discharge cycles, reaching a maximum value of 171.4 mAh g^{-1}, but that of electrode A increased to a maximum value of 228.5 mAh g^{-1} at the 81st cycle and then slowly decreased. During cycling, electrodes A and B showed higher specific capacity and better cycling stability than electrode C. To quantitatively characterize the cyclic stability of the nickel electrodes, the deterioration rate (R_d) is used, where R_d is equal to $(C_m - C_i)/C_m$ (C_m: maximum capacity; C_i: capacity at a certain cycle). The R_d at the 200th cycle for nickel electrodes A, B, and C are 8.09%, 11.4% and 32.2%, respectively, which indicates that the nickel hydroxide powders prepared by the new method have much better cyclic stability and higher discharge capacity than the powder obtained by the conventional co-precipitation method.

In summary, the non-spherical nickel hydroxide prepared by the new method has demonstrated not only a high tap-density, but also excellent electrochemical performance. Ramesh [38] reported that the better electrochemical activity is mainly dictated by structural disorder and is not associated with the tap-density of nickel hydroxide. However, these results clearly show that better electrochemical activity can be achieved by obtaining nickel hydroxide with a higher tap-density. That is, the nickel hydroxide powder with higher tap-density yields greater discharge capacity, greater volume capacity, higher discharge voltage, better high-rate capability and better cyclic stability. This electrochemical performance improvement is attributable to better reaction reversibility, a higher proton diffusion coefficient, and lower electrochemical impedance, as indicated by CV and EIS.

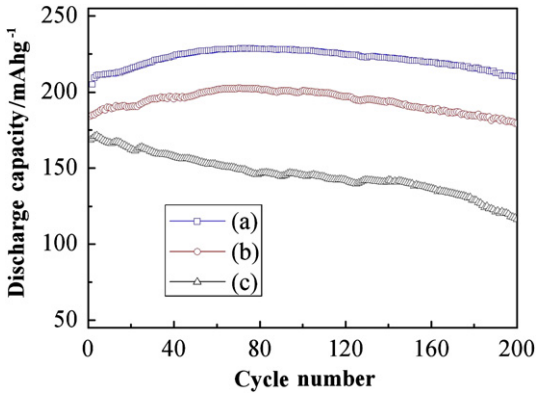

Fig. 10 – Cyclic performance of the electrodes prepared with samples A, B, and C at 1 C charge/discharge rate.

4. Conclusions

High-density, non-spherical nickel hydroxide was successfully synthesized by the PAM assisted two-step drying method. The tap-density of the powders thus obtained is 2.32 g cm^{-3}, which is notably higher than that of the nickel hydroxide powder obtained by the conventional co-precipitation method. The as-prepared nickel hydroxide materials have an irregular tabular shape, a high density of structural disorder, and a high specific surface area. The samples synthesized by the new method have better reaction reversibility, a higher proton diffusion coefficient, lower charge transfer resistance, higher specific capacity, higher volume capacity, and better cyclic stability than nickel hydroxide obtained by the conventional co-precipitation method. The results clearly show that better electrochemical activity can be achieved from nickel hydroxide with higher tap-density. We conclude that the PAM assisted two-step drying method is a simple, facile procedure for synthesizing non-spherical precursor powder that ultimately yields good performance and high tap-density in the final nickel hydroxide product.

Acknowledgements

This work is financially supported by the Natural Science Foundation of China under approval No. 20671031, and by Henan Provincial Department of Science and Technology Key Research Project under approval No.080102270013.

REFERENCES

[1] Geng M, Northwood DO. Development of advanced rechargeable Ni/MH and Ni/Zn batteries. Int J Hydrogen Energy 2003;28:633–6.
[2] Wu JB, Tu JP, Wang XL, Zhang WK. Synthesis of nanoscale CoO particles and their effect on the positive electrodes of nickel–metal hydride batteries. Int J Hydrogen Energy 2007; 32(5):606–10.
[3] Nathira Begum S, Muralidharan VS, Ahmed Basha C. The influences of some additives on electrochemical behaviour of nickel electrodes. Int J Hydrogen Energy 2009;34(3): 1548–55.

[4] Reisner David E, Salkind Alvin J, Strutt Peter R, Danny Xiao T. Nickel hydroxide and other nanophase cathode materials for rechargeable batteries. J Power Sources 1997;65:231–3.
[5] Chen J, Bradhurst DH, Dou S, Liu H. Nickel hydroxide as an active material for the positive electrode in rechargeable alkaline batteries. J Electrochem Soc 1999;146:3606–12.
[6] Chang ZR, Li GA, Zhao YJ, Chen JG, Ding YC. Influence of preparation conditions of spherical nickel hydroxide on its electrochemical properties. J Power Sources 1998;74:252–4.
[7] Wang XY, Yan J, Zhou Z, Lin J, Yuan HT, Song DY, et al. Electrochemical characteristics of nickel hydroxide modified by electroless cobalt coating. Int J Hydrogen Energy 1998;23 (10):873–8.
[8] Chang ZR, Tang HW, Chen JG. Surface modification of spherical nickel hydroxide for nickel electrodes. Electrochem Commun 1999;1:513–6.
[9] Yang CC. Synthesis and characterization of active materials of $Ni(OH)_2$ powders. Int J Hydrogen Energy 2002;27:1071–8.
[10] Ren JX, Yan J, Zhou Z, Wang XJ, Gao XP. High-temperature electrochemical performance of spherical $Ni(OH)_2$ coated with $Lu(OH)_3$. Int J Hydrogen Energy 2006;31:71–6.
[11] Zhang WG, Jiang WQ, Yu LM, Fu ZZ, Xia W, Yang ML. Effect of nickel hydroxide composition on the electrochemical performance of spherical $Ni(OH)_2$ positive materials for Ni–MH batteries. Int J Hydrogen Energy 2009;34(1):473–80.
[12] Acharya R, Subbaiah T, Anand S, Das RP. Preparation, characterization and electrolytic behavior of β-nickel hydroxide. J Power Sources 2002;109:494–9.
[13] Chen H, Wang JM, Pan T, Xiao HM, Zhang JQ, Cao CN. Effects of high-energy ball milling (HEBM) on the structure and electrochemical performance of nickel hydroxide. Int J Hydrogen Energy 2003;28:119–24.
[14] Song QS, Chiu CH, Chan SLI. Performance improvement of pasted nickel electrodes with an addition of ball-milled nickel hydroxide powder. Electrochim Acta 2006;51:6548–55.
[15] Song QS, Chiu CH, Chan SLI. Ball-milling processing of nanocrystalline nickel hydroxide and its effects in pasted nickel electrodes for rechargeable nickel batteries. J Solid State Electrochem 2008;12:133–41.
[16] Indira L, Dixit M, Kamath PV. Electrosynthesis of layered double hydroxides of nickel with trivalent cations. J Power Sources 1994;52(1):93–7.
[17] Watanabe K, Kumagai N. Thermodynamic studies of cobalt and cadmium additions to nickel hydroxide as material for positive electrodes. J Power Sources 1998;76: 167–74.
[18] Bernard MC, Cortes R, Keddam M, Takenouti H, Bernard P, Senyarich S. Structural defects and electrochemical reactivity of β-$Ni(OH)_2$. J Power Sources 1996;63(2):247–54.
[19] Deabate S, Fourgeot F, Henn F. X-ray diffraction and micro-Raman spectroscopy analysis of new nickel hydroxide obtained by electrodialysis. J Power Sources 2000;87: 125–36.
[20] Tessier C, Haumesser PH, Bernard P, Delmas C. The structure of $Ni(OH)_2$: from the ideal material to the electrochemically active one. J Electrochem Soc 1999;146(6):2059–67.
[21] Köhler U, Antonius C, Bäuerlein P. Advances in alkaline batteries. J Power Sources 2004;127:45–52.
[22] Ramesh TN, Vishnu Kamath P. The effects of stacking faults on the electrochemical performance of nickel hydroxide electrodes. Mater Res Bull 2008;43(11):2827–32.
[23] Balej J. Determination of the oxygen and hydrogen overcharge in concentrated alkali hydroxide solutions. Int J Hydrogen Energy 1985;10:365–74.
[24] Demourgues-Guerlou L, Delmas C. Structure and properties of precipitated nickel–iron hydroxides. J Power Sources 1993; 45(3):281–9.
[25] Zhao YL, Wang JM, Chen H, Pan T, Zhang JQ, Cao CN. Al substituted α-nickel hydroxide prepared by homogeneous precipitation method with urea. Int J Hydrogen Energy 2004; 29(8):889–96.
[26] Hu WK, Gao XP, Noréus D, Burchardt T, Nakstad NK. Evaluation of nano-crystal sized α-nickel hydroxide as an electrode material for alkaline rechargeable cells. J Power Sources 2006;160(1):704–10.
[27] Jeevanandam P, Koltypin Y, Gedanken A. Synthesis of nanosized α-nickel hydroxide by a sonochemical method. Nano Lett 2001;1(5):263–326.
[28] Kosova NV, Devyatkina ET, Kaichev VV. Mixed layered Ni–Mn–Co hydroxides: crystal structure, electronic state of ions, and thermal decomposition. J Power Sources 2007;174 (2):735–40.
[29] Portemer F, Delahaye-Vidal A, Figlarz M. Characterization of active material deposited at the nickel hydroxide electrode by electrochemical impregnation. J Electrochem Soc 1992;139 (3):671–8.
[30] Ramesh TN, Jayashree RS, Vishnu Kamathz P. The effect of the moisture content on the reversible discharge capacity of nickel hydroxide. J Electrochem Soc 2003;150:520–4.
[31] Liu B, Yuan H, Zhang Y, Zhou Z, Song D. Cyclic voltammetric studies of stabilized α-nickel hydroxide electrode. J Power Sources 1999;79:277–80.
[32] Zimmerman AH, Effa PK. Discharge kinetics of the nickel electrode. J Electrochem Soc 1984;131(4):709–13.
[33] Cao X, Wei J, Luo Y, Zhou Z, Zhang Y. Spherical nickel hydroxide composite electrode. Int J Hydrogen Energy 2000;25(7):643–7.
[34] Mancier V, Métrot A, Willmann P. AC impedance modelling of nickel hydroxide electrodes viewed as mixed protonic-electronic conductors. Electrochim Acta 1996;41:1259–65.
[35] Liu B, Yuan HT, Zhang YS. Impedance of Al-substituted α-nickel hydroxide electrodes. Int J Hydrogen Energy 2004;29: 453–8.
[36] Li YW, Yao JH, Liu CJ, Zhao WM, Deng WX, Zhong SK. Effect of interlayer anions on the electrochemical performance of Al-substituted α-type nickel hydroxide electrodes. Int J Hydrogen Energy 2010;35:2539–45.
[37] Chang ZR, Li HJ, Tang HW, Yuan XZ, Wang HJ. Synthesis of γ-CoOOH and its effects on the positive electrodes of nickel batteries. Int J Hydrogen Energy 2009;34:2435–9.
[38] Ramesh TN. The effect of tap density on the reversible charge storage capacity of nickel hydroxide electrodes. J Alloys Compd 2009;478:12–5.